arXiv:1512.02382v2 [physics.flu-dyn] 14 Aug 2016

Emergence of spatio-temporal dynamics from exact coherent solutions in pipe flow

Paul Ritter[1,2], Fernando Mellibovsky[3] and Marc Avila[1,2]
[1] *Institute of Fluid Mechanics, Friedrich-Alexander-Universität Erlangen-Nürnberg, 91058 Erlangen, Germany*
[2] *Center of Applied Space Technology and Microgravity, University of Bremen, 28359 Bremen, Germany*
[3] *Castelldefels School of Telecom and Aerospace Engineering, Universitat Politècnica de Catalunya, 08222 Barcelona, Spain*

(Dated: March 6, 2022)

Turbulent-laminar patterns are ubiquitous near transition in wall-bounded shear flows. Despite recent progress in describing their dynamics in analogy to non-equilibrium phase transitions, there is no theory explaining their emergence. Dynamical-system approaches suggest that invariant solutions to the Navier–Stokes equations, such as traveling waves and relative periodic orbits in pipe flow, act as building blocks of the disordered dynamics. While recent studies have shown how transient chaos arises from such solutions, the ensuing dynamics lacks the strong fluctuations in size, shape and speed of the turbulent spots observed in experiments. We here show that chaotic spots with distinct dynamical and kinematic properties merge in phase space and give rise to the enhanced spatio-temporal patterns observed in pipe flow. This paves the way for a dynamical-system foundation to the phenomenology of turbulent-laminar patterns in wall-bounded extended shear flows.

I. INTRODUCTION

Despite the ubiquity of turbulence, a theory explaining the emergence of its complexity has remained elusive even though the governing equations have been known for nearly two centuries. Landau [1] proposed in the 1940s that as the Reynolds number Re increases, turbulence arises through an infinite sequence of linear instabilities. In this picture each instability would add a new temporal frequency to the flow eventually resulting in the continuous spectrum that is characteristic of turbulence. Ruelle and Takens [2] refined this idea and established the current paradigm for the onset of turbulence: a few instabilities suffice to produce a continuous spectrum and render the flow chaotic. Such a scenario was first successfully demonstrated in laboratory experiments in a Taylor–Couette setup [3], and illustrations of other routes to chaos via period-doubling and intermittency followed shortly after [4]. This framework has been useful in explaining the origin of temporal chaos in many systems but falls short of describing turbulence because it fails to account for spatial features [5].

The importance of spatial interactions in fluid flows can be seen in pipes, channels and boundary layers already at low Re. In these and other wall-bounded shear flows turbulence first appears in isolated patches surrounded by laminar flow [6]. This coexistence is possible because the laminar flow is linearly stable and finite amplitude disturbances are needed to seed turbulence. In pipe flow the Reynolds number (defined as $\mathrm{Re} := DU/\nu$, with D the pipe diameter, U the constant mean driving speed and ν the kinematic viscosity of the fluid) is the sole governing parameter. Figure 1 illustrates the dynamics of a localised turbulent patch or puff in a 50-diameter long pipe at $\mathrm{Re} = 1860$. While the mass-flux is kept constant, the driving pressure gradient, the streamwise length of the turbulent region and its propagation speed strongly fluctuate, and the internal arrangement of high and low velocity streaks within the puff evolves erratically (see Fig. 1c). These spatio-temporal fluctuations result in the eventual collapse of the puff back to laminar flow in a memoryless decay process [7]. Although the characteristic lifetime of puffs increases with Re, puffs remain transient and their dynamics is consistent with a chaotic repeller or saddle in the phase space of the Navier–Stokes equations [8, 9]. However, as Re is increased, puffs can also expand in length and split [10], thereby progressively filling the pipe with a spatially intermittent laminar-turbulent pattern [11]. In the limit of long pipes, a self-sustained turbulent state first arises once the puff-splitting rate exceeds the decay rate [12], which happens at $\mathrm{Re} \approx 2040$. Recently, this transition type has been shown to belong to the universality class of directed percolation for Couette flow [13].

Despite recent progress in quantifying and modelling [14] the onset of turbulence in pipe flow as a spatio-temporal system whose fundamental units are puffs, surprisingly little is known about their origin. In fact, a framework providing a plausible explanation for their formation just begins to emerge. The key idea is that puffs stem from coherent structures (simple invariant solutions) of the Navier–Stokes equations that serve as elementary building blocks [15]. The simplest such structures in pipe flow are spatially periodic traveling waves [16], which are relative equilibria of the governing equations. More recently, streamwise localised solutions arising at a saddle-node bifurcation at $\mathrm{Re} = 1428$ have been found [17] (fig. 2). These solutions possess reflectional and π-rotational symmetry, and in this subspace the upper branch solution (UB in fig. 2) is stable up to $\mathrm{Re} = 1532.5$, which allows its computation directly by time-stepping of the Navier–Stokes equations. The lower branch solution (LB in fig. 2) has a single unstable direction and is an edge state [18] locally separating phase-space trajectories that turn chaotic from those that go laminar. At $\mathrm{Re} \approx 1533$ the upper-branch solution undergoes a subcritical Neimark–Sacker bifurcation, with a narrow hysteresis band down to $\mathrm{Re} = 1531.3$, followed

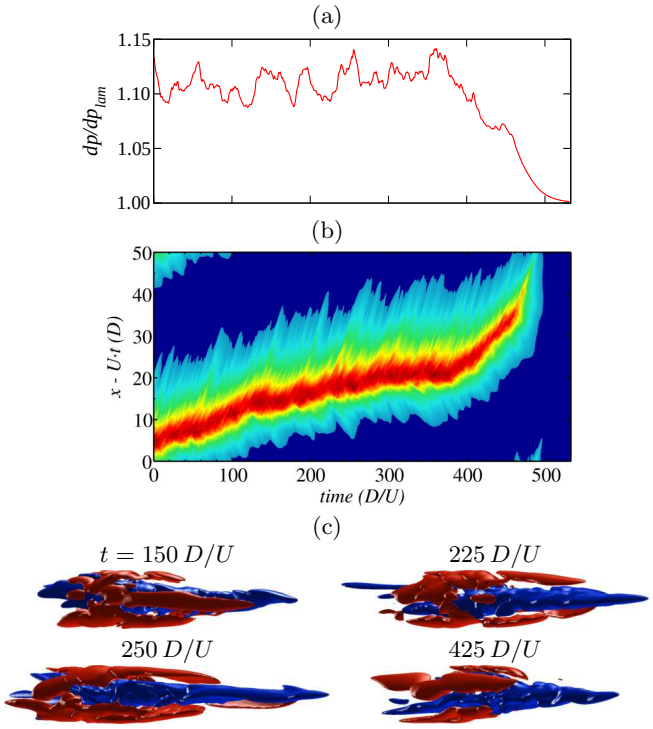


FIG. 1. Turbulent puff in pipe flow. (a) Time evolution of the pressure gradient required to drive a constant flow rate at Reynolds number Re = 1860, normalised with the value for laminar flow. (b) Space-time diagram of the energy (logarithmically scaled). The space axis is periodic and corresponds to a reference frame moving at the mean speed U of the flow. (c) Isosurfaces of streamwise velocity at $0.2\,U$ (red) and $-0.2\,U$ (blue). The laminar parabolic profile has been subtracted and the axial dimension scaled to aid visualisation.

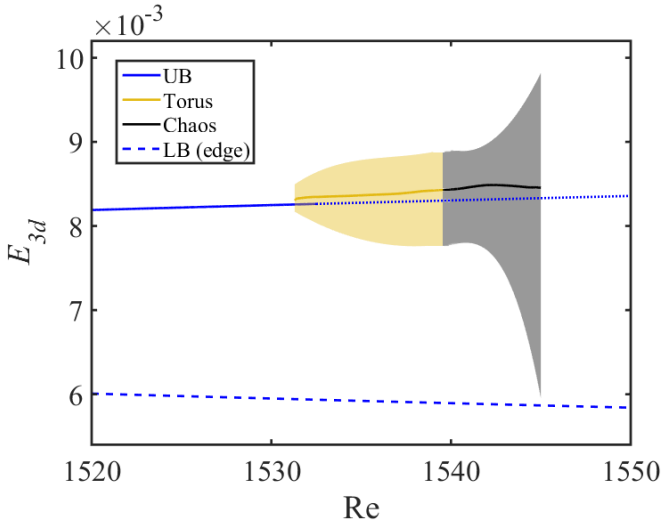


FIG. 2. Diagram of the time-averaged kinetic energy of the streamwise-dependent part of the velocity field $E_{3d} = ||\boldsymbol{v} - \langle \boldsymbol{v} \rangle_x||_2^2$ as a function of Reynolds number, depicting the saddle-node bifurcation in [17]. The stable upper branch solution (UB), a localised relative periodic orbit, turns into a torus (orange), which breaks up into a chaotic attractor (black). The shaded areas show the variation of energy over long runs. The chaotic fluctuations approach the lower branch solution (LB) separating chaos from the laminar state.

by break-up into chaos at Re = 1540. At Re $\gtrsim$ 1545 flow trajectories were observed to relaminarise, hinting at a global bifurcation turning the chaotic attractor into a chaotic saddle or repeller [17] (fig. 2). The dynamics of a relaminarising run at Re = 1546 is shown in Fig. 3. The corresponding spatially localised spot exhibits chaotic yet mild modulations of structure, streamwise length and propagation speed. It is referred to as "chaotic spot" in the rest of the paper in order to make clear that its behaviour is in contrast with the strong spatio-temporal fluctuations exhibited by turbulent puffs. This difference in spatio-temporal complexity, however, raises the question of what further qualitative changes occur in phase space as Re increases.

In this paper we show a mechanism increasing the spatio-temporal complexity of chaotic motions in pipe flow. As the Reynolds number is increased several chaotic saddles appear in phase space. Each of them is associated with localised spots with distinct propagation speed and streamwise length. Initially these saddles are rather isolated in phase space, but their successive merging results in trajectories that explore increasingly larger regions. In physical space, this translates into spot length and pres-

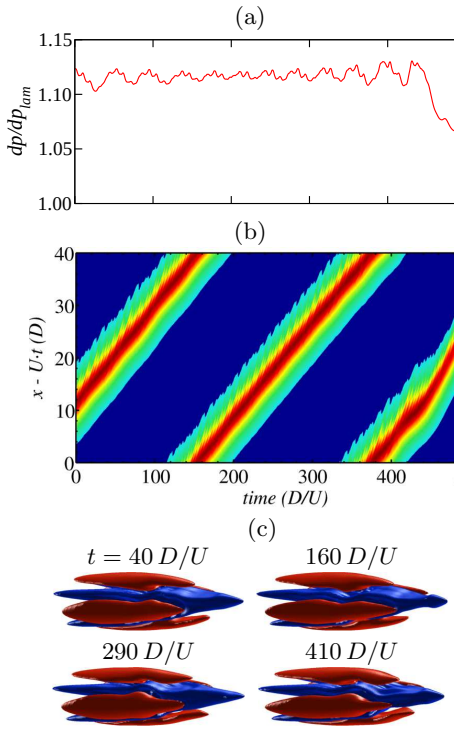


FIG. 3. (a) Time evolution of the normalised pressure gradient for a chaotic spot at Re = 1546. (b) Corresponding space-time diagram. (c) Isosurfaces of streamwise velocity; All axes and colouring as in Fig. 1.

sure fluctuations closer to those of turbulent puffs.

II. METHODS

In order to render the problem more tractable we simplify the dynamics by restricting them subject to reflectional symmetry about a diametrical plane and π-rotational periodicity with respect to the pipe axis, as in [17]. The only exception to this is Fig. 1, which was run in full space. Direct numerical simulations of the Navier–Stokes equations in cylindrical coordinates are carried out using the hybrid spectral finite-difference code of Willis [19], which is based on a velocity-potential formulation automatically satisfying the continuity equation and thereby avoiding the computation of the pressure. The coupled boundary conditions on the potentials are solved to machine precision with the influence-matrix method. We refer the interested reader to [19] for details.

We use periodic boundary conditions in the streamwise direction, with computational domains long enough (40 to 100 D) such that no interaction occurs between the upstream and downstream fronts of the turbulent patches. For $\mathrm{Re} < 1650$ we adopt a time-step $\delta t = 0.0025\, D/U$, 768 axial Fourier modes ($K = \pm 384$) for a length of 50 D, 32 azimuthal Fourier modes ($M = \pm 16$) for $\theta \in [0, \pi)$ and $N = 48$ points in the radial direction. This grid resolution and time-step allow us to determine the bifurcation sequence leading to transient chaos with a precision better than $\Delta\mathrm{Re} = \pm 1$. Both time-step and spatial discretisation are slightly finer than for previous simulations at larger Re in full space [9] that managed to achieve quantitative agreement with turbulent puffs lifetimes measured in extremely accurate and precisely controlled experiments [8]. For $\mathrm{Re} \geq 1650$ we use a domain length of 100 D and $K = \pm 1024$ to accurately resolve the increasingly turbulent dynamics.

III. BOUNDARY CRISIS TO TRANSIENT CHAOS

We start by analysing the transition from persistent to transient chaotic spots, which was previously estimated to occur at $\mathrm{Re} \gtrsim 1545$ [17]. In order to shed light on the underlying bifurcation mechanism, we perform a statistical study of the mean lifetime (τ) of the transients. Initial conditions for this study were taken from a chaotic spot at $\mathrm{Re} = 1545$. Figure 4a shows the survival probability of the transients as a function of elapsed time for several $\mathrm{Re} > 1545$. As in low-dimensional systems relaminarisation follows a memoryless decay characterised by the escape rate $1/\tau$ from a chaotic saddle [20]. As Re increases, the mean lifetime rapidly decreases and is well described by

$$\tau = \frac{a}{\mathrm{Re} - \mathrm{Re_{bc}}}, \qquad (1)$$

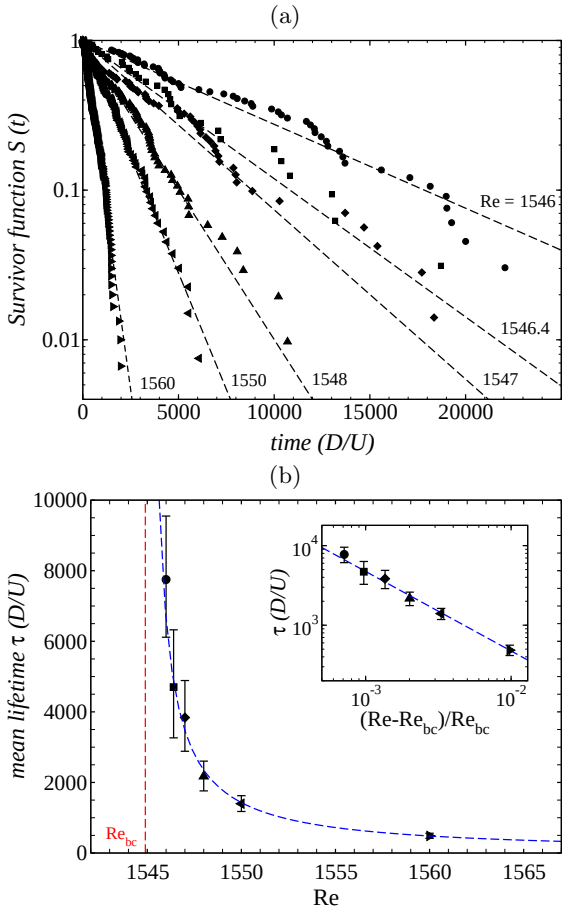


FIG. 4. (a) Survival probability of chaotic transients as a function of time for $\mathrm{Re} \in [1546, 1560]$. Initial conditions were taken from a chaotic spot at $\mathrm{Re} = 1545$. (b) Mean lifetime τ extracted from the distributions in (a), with the corresponding confidence intervals estimated as in [12]. The vertical (red) dashed line shows the critical Reynolds number $\mathrm{Re_{bc}} = 1545$. This was obtained with an inverse fit to equation (1), which is shown as a (blue) dashed line. The inset shows the lifetime scaling as function of reduced Reynolds number in log-log axes.

with critical Reynolds number $\mathrm{Re_{bc}} = 1545$ and $a = 7293\, D/U$ obtained from an inverse linear fit (blue dashed line in Fig. 4b and inset). Note that in experiments the lifetimes of turbulent puffs increase super-exponentially for $\mathrm{Re} > 1700$ [7], which suggests that further qualitative changes must occur in phase space as Re increases. The simple scaling of equation (1) is typical of low-dimensional chaos [20], and suggests that the onset of transients may take place via a generic mechanism called boundary crisis [21]. In a boundary crisis, the attractor collides with its own basin boundary and opens up to become a strange or chaotic saddle [20].

This hypothesis is put to test here by examining the behaviour of extremely long phase-space trajectories ($> 10^5\, D/U$) of the attractor in the range $\mathrm{Re} \in [1540, 1545]$. Fig. 5 shows that the chaotic trajectories sporadically

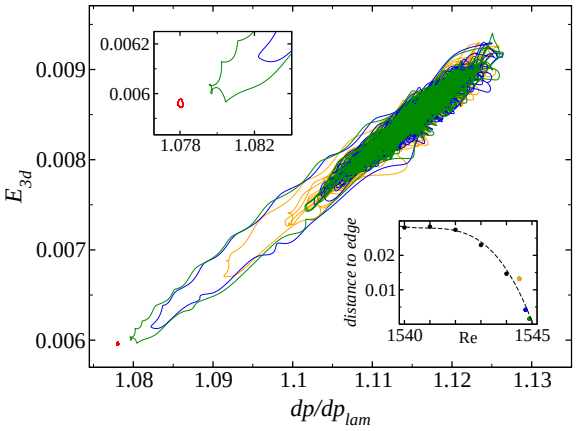


FIG. 5. Phase-portrait of the chaotic attractor at Re = 1544.5 (orange), 1544.75 (blue) and 1544.9 (green). The dynamics are projected onto a two-dimensional plane defined by the normalised pressure gradient dp/dp_{lam} and the kinetic energy of the streamwise-dependent part of the velocity field E_{3d}. The trajectories approach the "edge state" on the basin boundary of the attractor, which is shown in red. The upper-left inset shows a closeup near the edge state. The bottom right inset shows how the distance between the attractor and its basin boundary (as defined by minimum pressure gradient difference with the edge state over time) goes to zero as $\mathrm{Re}_{\mathrm{bc}} = 1545$ is approached. The dashed line helps to guide the eye (cubic fit to the data).

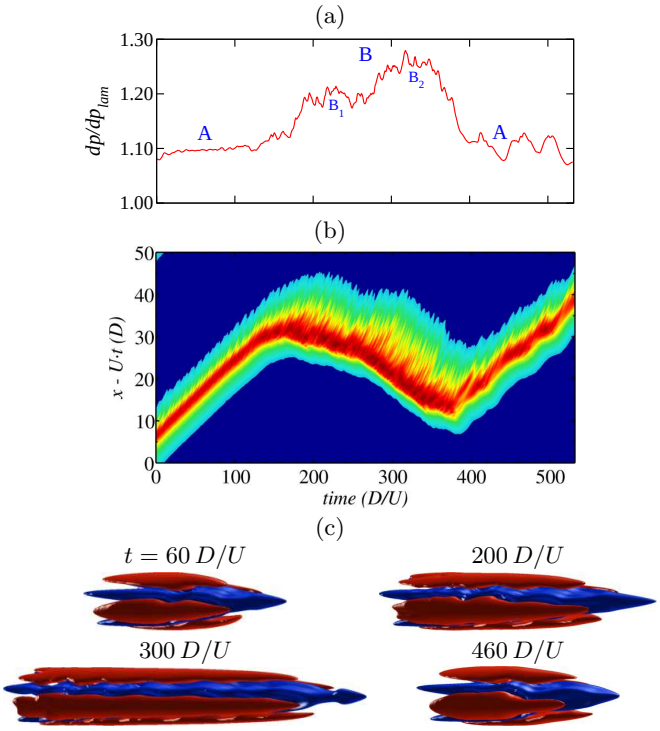


FIG. 6. Emergence of turbulent dynamics from interacting chaotic spots. At Re = 1580 the flow exhibits sudden changes in dynamical and kinematic properties before relaminarising. These occur through the interaction of two chaotic saddles corresponding to short (A) and long (B) chaotic spots. (a) Excerpt of a trajectory. (b) Corresponding space-time diagram. (c) Isosurfaces of streamwise velocity; All axes and coloring as in Fig. 1.

visit the neighbourhood of the lower branch solution, which is known to be the attractor at the basin boundary (or edge state [18]) in the subspace [17]. The edge state is visited more closely with increasing Re and, as $\mathrm{Re}_{\mathrm{bc}}$ is approached, the minimum distance to the edge state vanishes (bottom-right inset of Figure 5). This trend supports the boundary crisis hypothesis and a cubic fit to the data yields $\mathrm{Re}_{\mathrm{bc}} = 1545$, exactly as for the lifetimes analysis. Crises leading to chaotic transients were recently observed in Couette [22], channel [23] and pipe flows [24], highlighting their ubiquity in shear flows. Note however that all these studies were done in short periodic domains unable to capture spatial localisation, a salient feature of shear flow turbulence.

IV. ONSET OF SPATIO-TEMPORAL FLUCTUATIONS VIA SADDLE MERGER

The mild fluctuations displayed by the transient chaotic spot together with the simple lifetime scaling suggest that the dynamics involved is low-dimensional. However, traces of more complex behaviour can be observed at larger Re. Figure 6a shows the time evolution of the driving pressure gradient corresponding to a run at Re = 1580, which was initialised from a chaotic spot at Re = 1545 and relaminarises at a later time (not shown). Initially the dynamics remains on a low friction plateau (labelled "A"), and the spot has a streamwise length and propagation speed similar to that observed at lower Re. This is evidenced by comparison of the space-time diagram of Fig. 6b up to $t = 150\,D/U$, to its counterpart at Re = 1546 (Fig. 3b). Subsequently the dynamics explores a region of higher friction (labelled "B"), which corresponds to a spatial expansion of the spot (see the snapshots of Fig. 6c). Thereafter the spot rapidly recedes in length and the dynamics settles anew on the low friction plateau A.

The phase portraits of Fig. 7 illustrate the dynamics of the flow for several Re. At Re = 1546 the dynamics revolves around a fairly small region of phase space (A), whereas a much larger region is explored at Re = 1580. This qualitative change suggests that two separate regions of phase space, (A) and (B), originally dynamically isolated, have merged at a global bifurcation. The chaotic spot that results from the merger exhibits strong fluctuations in its propagation speed and spatial extent (see Fig. 6b–c)). To elucidate the nature of the underlying global bifurcation we perform an additional set of runs with initial conditions taken from a turbulent flow at larger Re = 2000, thus ensuring that the dynamics are not biased to start from too close to A.

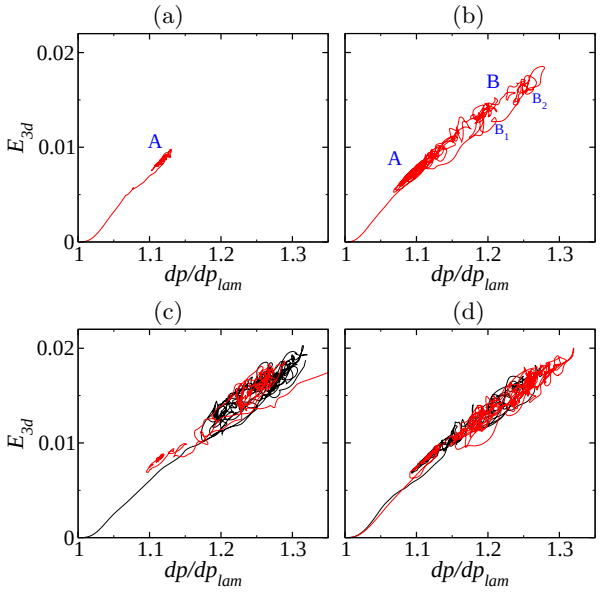


FIG. 7. Phase portraits in the vicinity of the boundary crisis ($Re_{bc} \approx 1545$). (a) Dynamics slightly after the crisis (Re = 1546, run of Fig. 3) and (b) far beyond the crisis (Re = 1580, run of Fig. 6). Initial conditions for (a,b) are taken from a chaotic spot at Re = 1545. (c) Dynamics prior to the crisis (Re = 1540): one trajectory starts in region B and evolves towards A where it stays forever (red) while the other relaminarises directly from region B (black). (d) Dynamics after the crisis (Re = 1550): one trajectory relaminarises from region A after having visited B (red) whereas the other relaminarises from B after having visited A (black). Initial conditions for (c,d) are taken from a turbulent puff at Re = 2000.

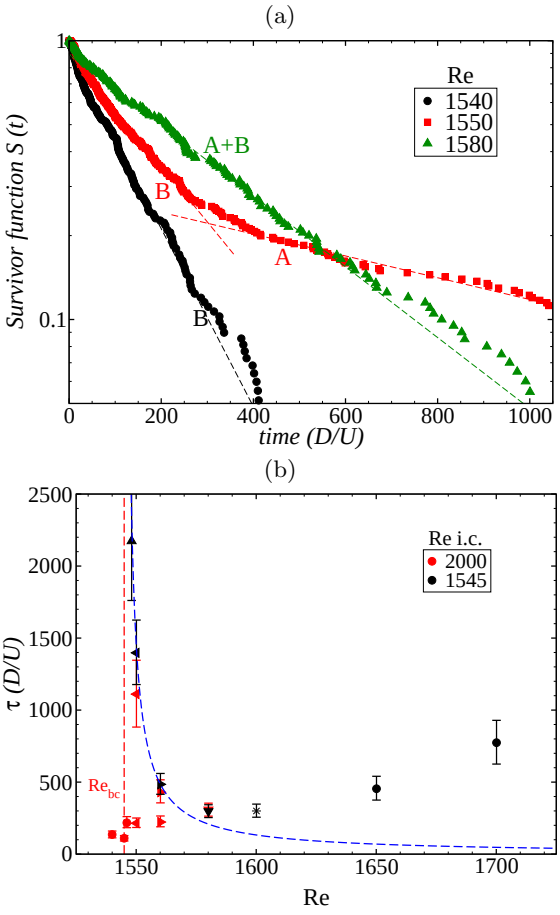


FIG. 8. (a) Survival probability obtained from initial conditions at Re = 2000. The data at Re = 1550 (red) exhibits two slopes, which reflect the interaction of two merging chaotic saddles (A and B). (b) Mean lifetime extracted using initial conditions from either the chaotic saddle A at Re = 1545 (black, same data as in Fig. 4b) or turbulent flow at Re = 2000 (red, see distributions in (a)).

A. Dynamics prior to the boundary crisis

We first reduce the Reynolds number from Re = 2000 to Re = 1540, which precedes the boundary crisis ($Re_{bc} = 1545$). Here A is an attractor and phase-space trajectories evolving towards it remain there forever (see the red curve in Fig. 7c). Other trajectories approach region B instead before finally relaminarising (black curve). Of a total of 300 such runs, 22% converged onto A (either directly or after an interim visit to B) while the remaining 78% visited B before relaminarising. The survivor function of the latter is marked with black symbols in Fig. 8a, and its exponential trend confirms the existence of a second saddle B.

Figure 7c shows that B holds transient dynamics that eventually leave towards either laminar flow (black curve) or coexisting attractor A (red curve). Following the boundary crisis, A also becomes a saddle and all trajectories ultimately relaminarise regardless of whether they temporarily settled on either A or B (Fig. 7d).

B. Weak saddle interaction after the crisis

At slightly larger Re = 1550 trajectories occasionally switch between the two saddles (Fig. 7d), which supports that saddles A and B have undergone a merging crisis [25]. Visits to both A and B are rare and two slopes, corresponding to either saddle, are clearly discernible in the survivor function for Re = 1550 (red symbols in Fig. 8a). The points on the right slope correspond to trajectories that evolve towards A and have longer lifetimes than those that approach B (left slope). Note that pinpointing the precise Re at which the merger takes place would require substantially longer runs and finer Re-steps than are feasible in reasonable time scales. However, our data suggests that the merger occurs very closely, if not immediately, after the boundary crisis. The combined saddle features enhanced spatio-temporal chaos.

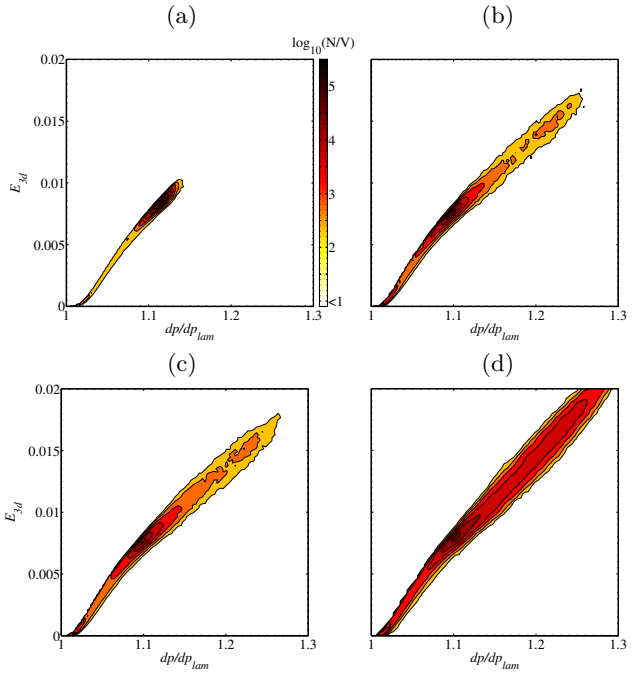


FIG. 9. Phase space histograms (logarithmically scaled) of all runs at various Re with initial conditions at Re = 1545. N/V is the count normalized with the volume of the histogram. (a) Re = 1550. (b) Re = 1580. (c) Re = 1600. (d) Re = 1650.

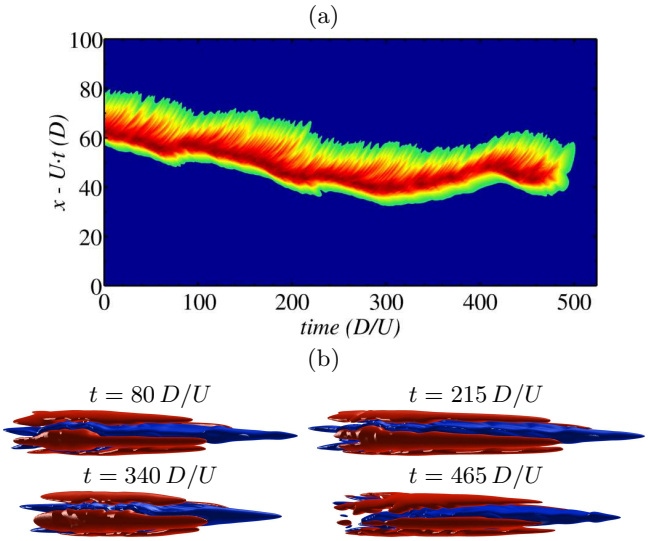


FIG. 10. (a) Space-time diagram and (b) streamwise velocity isosurfaces at Re = 1700; Axes and colouring as in Fig. 1.

C. Progressive merger of saddles

As Re is further increased the ghosts of the two saddles progressively blend into one sole entity (Fig. 9). At Re $\approx$ 1580 the characteristic times for transitions between A and B become shorter than their relaminarisation times, so most trajectories visit both A and B several times before relaminarising (see Figs. 6 and 7b). Henceforth the two saddles effectively become one and most phase-space trajectories explore the total phase space associated beforehand with A and B (see Figs. 7b, 7d and 9b). As a consequence, a unique combined slope emerges in the survival function (green symbols in Fig. 8a). As the transition rate among saddles increases, the clearly identifiable regimes of Fig. 6 gradually transform into the puff-like dynamics of Figs. 10a–b. The merger in phase space is accompanied by a rise in lifetimes with increasing Re (Fig. 8b) as trajectories bounce from saddle to saddle more and more frequently. This reverses the initial decreasing trend followed after the boundary crisis and is thus consistent with experimental observations [7, 8].

Kreilos *et al.* [26] have also reported a mechanism increasing the lifetimes of chaotic transients. In their simulations of minimal-flow-unit plane Couette flow an attractor arises within an existing saddle. The attracting bubble bursts in a crisis and the new saddle features its own lifetime statistics, which differ from those of the pre-existing saddle. As a result, the combined ensuing lifetimes increase in a non-smooth and non-monotonic fashion, which is in stark contrast to the monotonous increase of lifetimes that follows the saddle merger observed here.

D. Bifurcation mechanisms behind saddle merger

In the last decade several PDE-based models with at least one spatial extended dimension have been employed to illustrate the behaviour of chaotic saddles in high-dimensional dynamical systems [27]. Particular attention has been paid to the type of crises leading from temporal to spatio-temporal chaos [20, 28]. Despite the important role of chaotic saddles in these models, their ensuing spatio-temporal chaos is always attracting. The underlying attractor results from an interior crisis of a temporally chaotic attractor evolved from a saddle node bifurcation. The spatio-temporal dynamics are already encoded in the surrounding chaotic saddle within which the interior crisis occurs, but since the only leak of the saddle is towards the embedded attractor, the resulting set is an enlarged spatio-temporally chaotic attractor that encompasses the pre-existing attractor and saddle. The scenario changes dramatically whenever the basin boundary separating laminar flow from the second attractor has previously undergone a smooth-fractal and, possibly, subsequent fractal-fractal metamorphoses [29]. Then a direct transition from permanent temporal chaos to transient spatio-temporal chaos becomes feasible [30].

A general theory relating crises of chaotic sets, basin boundary metamorphoses and explosions of chaotic saddles [31] sets the framework in which our results may be interpreted. Upon the genesis of saddle A in a boundary crisis no permanent dynamics remain. The explosion of attractor A into saddle A+B and the pre-existence of saddle B suggest that the crisis involves a fractal basin boundary, much as in [28, 32], except that the resulting

spatio-temporal chaotic set is a saddle instead of an attractor. The fact that spatio-temporally chaotic saddle B can drive trajectories indistinctly towards A or laminar flow, indicates that it is embedded in the basin boundary, which is fractal. As the boundary crisis occurs and temporal chaotic attractor A becomes a saddle, A is subsumed into an enlarged spatio-temporal chaotic saddle A+B within the basin boundary. At low Re the basin boundary is smooth and presumably becomes fractal in a smooth-fractal metamorphosis [29]. This metamorphosis might be related to the very creation of saddle B, which would have emerged within the basin boundary or fused with it in its own crisis. Note that unlike for shear flows none of the aforementioned studies on PDE-based models involves localised structures.

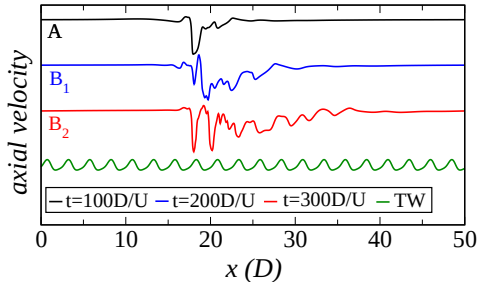


FIG. 11. Axial velocity distribution along a streamwise line at $(r, \theta) = (0.2\,D, 0)$ of the flow snapshots in Fig. 6c and the traveling wave $N2$ found by Pringle *et al.* [33] (Re = 2400, axial wavelength $2.513\,D$)

V. ORIGIN OF CHAOTIC SADDLES

In §III we have demonstrated that saddle A emerges as the chaotic attractor grows and finally collides with its basin boundary at $\mathrm{Re}_{\mathrm{bc}} = 1545$. This raises the question of whether saddle B results from a similar global bifurcation. Note however that the dynamics of B is much more complex than that of A: in Figure 6b two distinct friction plateaus (B_1 and B_2) are clearly discernible within B, and the phase portrait of Fig. 7b also shows that the dynamics of B_1 and B_2 unfolds in two distinct regions of phase space. The space-time diagram of Fig. 6b and snapshots of streamwise velocity isosurfaces in Fig. 6b–c further evidence, now in physical space, that B_1 and B_2 correspond to two spots with different streamwise length and propagation speed.

In an attempt to elucidate the origin of saddle B, we performed an extensive study of its lifetimes statistics. Interestingly, at $\mathrm{Re} \sim 1470$ lifetime distributions feature two clear slopes corresponding to spots B_1 and B_2. These are similar to the lifetime distribution shown as red in Fig. 8a and hence not shown here. For $\mathrm{Re} \gtrsim 1470$, a single slope is observed in the lifetime statistics, which indicates that B_1 and B_2 have merged to form B. We further reduced the Reynolds number in an attempt to detect the initiation of the merger, but this resulted in the sudden disappearance of B at around $\mathrm{Re} \sim 1450$, suggesting that, unlike what happens with A and B at higher Re, the dynamics associated with the independent B_1 and B_2 saddles is highly unstable and only becomes detectable upon their merging to form B. Altogether, the dynamics in the range $1460 < \mathrm{Re} < 1540$ is extremely complex and beyond the scope of this work.

Recently, Chantry *et al.* [34] showed that the localised relative periodic orbit underlying saddle A emerges from a spatially periodic travelling wave (named $N2$) at a subharmonic Hopf bifurcation. Figure 11 shows the streamwise velocity along an axial line for $N2$ and for the flow snapshots of Fig. 6c. The internal wave structure of snapshots of B_1 and B_2, consisting of wave trains of different lengths, is also strikingly reminiscent of $N2$. Despite this similarity we could not determine whether exact solutions underlying B_1 and B_2 also stem from $N2$ or other traveling-wave solutions. A Newton-Krylov solver specially devised to compute relative periodic solutions invariably failed to converge from any of the many snapshots of B_1 and B_2 that we seeded as initial guesses.

In planar shear flow spanwise localisation has been shown to follow homoclinic snaking [35], which generates multiple spanwise-localised solutions spanning different counts of vortex-pairs [36]. Although an analogous mechanism may generate localised relative periodic orbits that underlie A, B_1 and B_2, Mellibovsky and Meseguer [37] have recently demonstrated in the case of channel flow that the snaking mechanism is decisively disrupted in the streamwise direction. It was found instead that streamwise-localised relative periodic orbits of quantised lengths, exactly as the chaotic spots found here, appear in saddle-node bifurcations and extend to very high Re. These solutions are related by intricate connections in parameter space and by heteroclinic connections in phase space. We speculate that this type of solutions might set the stage for bifurcation cascades into chaotic attractors, and for the basin boundary metamorphoses and crises that finally result in the complexity of wall-bounded turbulent flows.

VI. CONCLUSION

Several routes to chaos were proposed in the seventies to account for the emergence of disordered dynamics in systems far from equilibrium [2, 4, 38]. These routes were first illustrated in simple dynamical systems and later observed in fluid experiments featuring linearly unstable laminar flows [3, 4]. More recently, numerical studies in small computational domains have shown that the same routes apply to linearly stable flows [22–24], albeit with decisive differences. First, the bifurcation cascade leading to chaos cannot start from laminar flow, and stems instead from disconnected invariant solutions originated at saddle-node bifurcations. These solutions are typically unstable in full space, so that all aforementioned

numerical investigations rely on restricting the dynamics to symmetry subspaces that stabilise them. A second essential difference is that shear flow turbulence is transient, which requires a transition from permanent to transient chaos as Re increases. While many numerical studies of shear flows in small domains have demonstrated the emergence of chaotic saddles, the associated transients invariably produce decreasing lifetimes for increasing Re. Experimental turbulent lifetimes rapidly surge instead, such that additional qualitative changes must take place in phase space. Finally, transitional shear flow turbulence is spatially localised and it is only through spatial proliferation of spots that turbulence becomes self-sustained [12, 39]. None of the theoretical and numerical studies cited takes this important spatial aspect into consideration, the former using models based on low-dimensional ODEs and maps, the latter employing numerical domains too small to capture localisation.

The first reported bifurcation cascade in a spatially extended shear flow, Hagen-Poiseuille flow in a long cylindrical pipe [17], laid out a two-step transition of a streamwise localised relative periodic orbit into a localised chaotic spot. Here we have shown that a boundary crisis in which the attractor collides with its own basin boundary is responsible for the transition from permanent to transient chaos. After the boundary crisis, lifetimes decrease rapidly with increasing Re following the simplest possible scaling law in low dimensional dynamical systems [40]. The dynamics of the resulting transient spot is only mildly chaotic, involving but weak fluctuations of pressure drop, propagation speed and length, typical of merely temporal chaos. We have shown that strong spatio-temporal chaotic fluctuations arise from a progressive merger of temporally chaotic saddles in phase space. Each saddle is associated with a chaotic spot of distinct characteristic streamwise length, propagation speed and pressure drop, such that their merger results in a spot whose length oscillates erratically. Completion of the saddles merger is followed at higher Re by phenomena typically observed in experiments [7] such as rapid lifetime growth with increasing Reynolds number (see Fig. 8b) or the enhancement of spatio-temporal fluctuations through an increase in the transition rate between the phase space regions originally occupied by isolated saddles. Overall, the dynamics after the merger is consistent with that of the turbulent puff. Furthermore, a spatial mechanism of occasional violent growth appears to be a precursor to splitting, which we have observed to start occurring at larger Re $\gtrsim 1700$ (see Fig. 12). Increasing lifetimes and spatial expansion of spots set the basis for an analogy between turbulent transition and directed percolation [13, 41], thus rendering our work relevant to future development of a rational foundation for this phenomenology.

A multitude of streamwise periodic travelling waves with different symmetries have been found in the last decade. These waves only require subharmonic bifurcations that have been shown to be generic [34] to produce streamwise localised solution branches that could, in turn, give rise to temporally chaotic saddles. Hence, analogous scenarios will most probably be at play within symmetry subspaces other than that considered here. Piecing together the progress made in different subspaces in order to explain the complexity observed in full space remains however an outstanding challenge. It is unclear as of today how to tackle the problem in the abscence of symmetry restrictions given that the localised edge state in full space is chaotic at all Reynolds numbers hitherto investigated [42, 43]. A quantitative characterisation of the progressive complexification of the dynamics, namely through the analysis of the evolution of the Lyapunov spectrum of spatio-temporal transients (see [44] for an application to coupled-map lattices), is beyond the scope of this work and therefore left for future study.

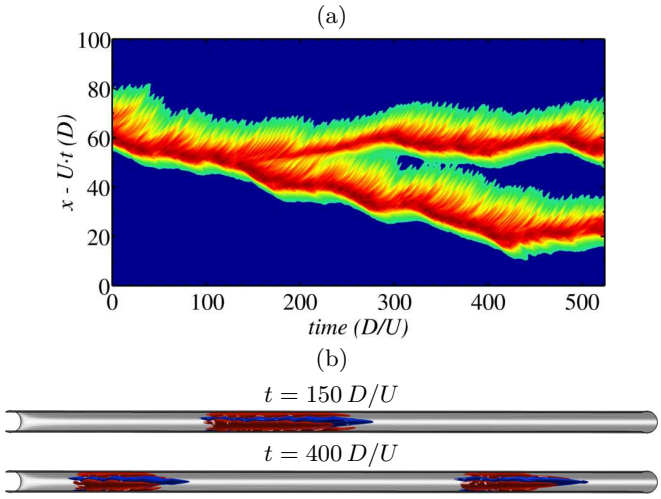


FIG. 12. (a) Space-time diagram and (b) streamwise velocity isosurfaces at Re = 1800 showing a splitting event; Axes and colouring as in Fig. 1.

Beyond the example of pipe flow, we expect our findings to be relevant also for flows with two spatially extended directions, such as channel and Couette flows. In these cases turbulence appears in the form of patches that are localised in both the streamwise and spanwise directions [6] and that feature yet richer spatial self-organisation processes [45]. Despite the challenge, doubly-localised invariant solutions have recently been discovered in these geometries [46] and are promising candidates for building blocks of turbulent dynamics in doubly-extended systems. More generally, the mechanisms shown here may be relevant to other extended systems driven far from equilibrium. In particular, we expect our route to complexity to be generic in excitable media, for which theories of temporal chaos also fail to properly characterise the spatio-temporal dynamics observed.

ACKNOWLEDGMENTS

Support from the Deutsche Forschungsgemeinschaft (DFG) through grant FOR 1182 and computing time from the Jlich Supercomputing Centre (grant number HER22) and Regionales Rechenzentrum Erlangen (RRZE) are acknowledged. FM (Serra Húnter fellow) also acknowledges financial support from grants FIS2013-40880-P and 2014SGR1515 from the Spanish and Catalan governments, respectively.

[1] L. D. "Landau, "CR Acad. Sci. URSS" **"44"**, "1 ("1944").

[2] D. Ruelle and F. Takens, Commun. Math. Phys. **20**, 167 (1971); S. Newhouse, D. Ruelle, and F. Takens, Communications in Mathematical Physics **64**, 35 (1978).

[3] J. P. Gollub and H. L. Swinney, Phys. Rev. Lett. **35**, 927 (1975).

[4] M. J. Feigenbaum, Journal of statistical physics **19**, 25 (1978); Y. Pomeau and P. Manneville, Communications in Mathematical Physics **74**, 189 (1980); J.-P. Eckmann, Reviews of Modern Physics **53**, 643 (1981); A. Libchaber, C. Laroche, and S. Fauve, Journal de Physique Lettres **43**, 211 (1982).

[5] H. Chaté and P. Manneville, Phys. Rev. Lett. **58**, 112 (1987).

[6] O. Reynolds, Proc. Roy. Soc. London **35**, 84 (1883); H. W. Emmons, J. Aero. Sci. **18**, 490 (1951); N. Tillmark and P. H. Alfredsson, J. Fluid Mech. **235**, 89 (1992); G. Lemoult, J.-L. Aider, and J. E. Wesfreid, Journal of Fluid Mechanics **731**, R1 (2013).

[7] H. Faisst and B. Eckhardt, J. Fluid Mech. **504**, 343 (2004); B. Hof, J. Westerweel, T. Schneider, and B. Eckhardt, Nature **443**, 59 (2006); J. Peixinho and T. Mullin, Phys. Rev. Lett. **96**, 094501 (2006).

[8] B. Hof, A. De Lozar, D. Kuik, and J. Westerweel, Phys. Rev. Lett. **101**, 214501 (2008).

[9] M. Avila, A. Willis, and B. Hof, J. Fluid Mech. **646**, 127 (2010).

[10] I. J. Wygnanski, M. Sokolov, and D. Friedman, J. Fluid Mech. **69**, 283 (1975).

[11] D. Moxey and D. Barkley, Proc. Natl. Acad. Sci. USA **107**, 8091 (2010).

[12] K. Avila, D. Moxey, A. De Lozar, M. Avila, D. Barkley, and B. Hof, Science **333**, 192 (2011).

[13] G. Lemoult, L. Shi, K. Avila, S. V. Jalikop, M. Avila, and B. Hof, Nature Physics **12**, 254 (2016).

[14] D. Barkley, Phys. Rev. E **84**, 016309 (2011); M. Sipos and N. Goldenfeld, Phys. Rev. E **84**, 035304 (2011); K. T. Allhoff and B. Eckhardt, Fluid Dynam. Res. **44**, 031201 (2012); C. Marschler and J. Vollmer, SIAM J. Appl. Dyn. Syst. **13**, 1137 (2014); H.-Y. Shih, T.-L. Hsieh, and N. Goldenfeld, Nature Physics. **12**, 245 (2016).

[15] R. R. Kerswell, Nonlinearity **18**, R17 (2005); J. Gibson, J. Halcrow, and P. Cvitanović, J. Fluid Mech. **611**, 107 (2008); G. Kawahara, M. Uhlmann, and L. van Veen, Ann. Rev. Fluid Mech. **44**, 203 (2012).

[16] H. Faisst and B. Eckhardt, Phys. Rev. Lett. **91**, 224502 (2003); H. Wedin and R. R. Kerswell, J. Fluid Mech. **508**, 333 (2004).

[17] M. Avila, F. Mellibovsky, N. Roland, and B. Hof, Phys. Rev. Lett. **110**, 224502 (2013).

[18] J. D. Skufca, J. A. Yorke, and B. Eckhardt, Phys. Rev. Lett. **96**, 174101 (2006); T. M. Schneider, B. Eckhardt, and J. A. Yorke, Phy. Rev. Lett. **99**, 034502 (2007).

[19] A. P. Willis and R. R. Kerswell, J. Fluid Mech. **619**, 213 (2009).

[20] T. Tél and Y.-C. Lai, Phys. Rep. **460**, 245 (2008); T. Tél, Chaos **25**, 097619 (2015).

[21] C. Grebogi, E. Ott, F. Romeiras, and J. A. Yorke, Phys. Rev. A **36**, 5365 (1987).

[22] T. Kreilos and B. Eckhardt, Chaos **22**, 047505 (2012); M. Shimizu, G. Kawahara, J. Lustro, and L. van Veen, 11^{th} World Congress on Computational Mechanics (2014).

[23] S. Zammert and B. Eckhardt, Physical Review E **91**, 041003(R) (2015).

[24] S. Altmeyer, A. Willis, and B. Hof, arXiv preprint arXiv:1501.01989 (2015).

[25] J. Feng and W. Xu, Acta Phys. Sin. **60**, 080502 (2011).

[26] T. Kreilos, B. Eckhardt, and T. M. Schneider, Phys. Rev. Lett. **112**, 044503 (2014).

[27] E. Rempel and A. Chian, Phys. Lett. A **319**, 104 (2003); Chaos **14**, 545 (2003).

[28] E. Rempel and A. Chian, Phys. Rev. Lett. **98**, 014101 (2007); Phys. Rev. E **76**, 056217 (2007).

[29] C. Grebogi, E. Ott, and J. A. Yorke, Phys. Rev. Lett. **56**, 1011 (1986); Physica D **24**, 347 (1987).

[30] A. Chian, P. Muñoz, and E. Rempel, Phys. Rev. E **88**, 052910 (2013).

[31] C. Robert, K. Alligood, E. Ott, and J. A. Yorke, Physica D **144**, 44 (2000).

[32] E. Rempel, R. Miranda, and A. Chian, Phys. Fluids **21**, 074105 (2009).

[33] C. C. T. Pringle, Y. Duguet, and R. R. Kerswell, Phil. Trans. Roy. Soc. Lond. A **367**, 457 (2009).

[34] M. Chantry, A. P. Willis, and R. R. Kerswell, Phys. Rev. Lett. **112**, 164501 (2014).

[35] J. Burke and E. Knobloch, Phys. Lett. A **360**, 681 (2007).

[36] T. M. Schneider, D. Marinc, and B. Eckhardt, J. Fluid Mech. **646**, 441 (2010).

[37] F. Mellibovsky and A. Meseguer, J. Fluid Mech. **779**, R1 (2015).

[38] M. C. Cross and P. C. Hohenberg, Rev. Mod. Phys. **65**, 851 (1993).

[39] L. Shi, M. Avila, and B. Hof, Phys. Rev. Lett. **110**, 204502 (2013).

[40] C. Grebogi, E. Ott, and J. A. Yorke, Phys. Rev. Lett. **57**, 1284 (1986).

[41] Y. Pomeau, Physica D **23**, 3 (1986).

[42] F. Mellibovsky, A. Meseguer, T. M. Schneider, and B. Eckhardt, Phys. Rev. Lett. **103**, 054502 (2009).

[43] Y. Duguet, A. P. Willis, and R. R. Kerswell, J. Fluid Mech. **663**, 180 (2010).

[44] K. Kaneko, Physica D: Nonlinear Phenomena **34**, 1 (1989).

[45] Y. Duguet and P. Schlatter, Phys. Rev. Lett. **110**, 034502 (2013).

[46] E. Brand and J. F. Gibson, J. Fluid Mech. **750**, R3 (2014); S. Zammert and B. Eckhardt, Journal of Fluid Mechanics **761**, 348 (2014).